frontiers | Frontiers in Materials

TYPE Original Research
PUBLISHED 09 October 2023
DOI 10.3389/fmats.2023.1272147

OPEN ACCESS

EDITED BY
Robert Li,
City University of Hong Kong, Hong Kong SAR, China

REVIEWED BY
Enrique Cuan-Urquizo,
Monterrey Institute of Technology and Higher Education (ITESM), Mexico
Mingjun Hu,
Beihang University, China

*CORRESPONDENCE
Erik Kornfellner,
erik.kornfellner@meduniwien.ac.at

RECEIVED 03 August 2023
ACCEPTED 19 September 2023
PUBLISHED 09 October 2023

CITATION
Kornfellner E, Königshofer M, Unger E and Moscato F (2023), Elastic and dimensional properties of newly combined 3D-printed multimaterials fabricated by DLP stereolithography. *Front. Mater.* 10:1272147. doi: 10.3389/fmats.2023.1272147

Elastic and dimensional properties of newly combined 3D-printed multimaterials fabricated by DLP stereolithography

Erik Kornfellner[1]*, Markus Königshofer[1], Ewald Unger[1] and Francesco Moscato[1,2,3]

[1]Center for Medical Physics and Biomedical Engineering, Medical University of Vienna, Vienna, Austria, [2]Ludwig Boltzmann Institute for Cardiovascular Research, Vienna, Austria, [3]Austrian Cluster for Tissue Regeneration, Vienna, Austria

In the field of stereolithography 3D printing, the portfolio of commercially available photopolymers has burgeoned. Each material family possesses its individual properties. However, corresponding products with specific requirements remain a major challenge. This gap could be filled by combining existing materials. This study aimed to predict Young's modulus of the specimen manufactured by combining multiple materials using digital light processing (DLP), a subtype of stereolithography. It also aimed to investigate the effects of the printing process on the geometry and mechanical properties of such 3D-printed multimaterials. Using a DLP 3D printer, samples were produced from commercially available pure and mixed materials, and half of the samples underwent post-printing curing. Three-point bending tests were performed to determine the elastic modulus of the samples. The elastic properties have been compared to linear interpolation using the properties of the primary materials. The measurements showed that Young's modulus ranged from 1.6 GPa to 2.2 GPa for the post-cured materials, with the mixed materials fitting well with the linear interpolation approach. For eight out of nine sample sets, the prediction was within the range of the measurements. In the case of as-printed samples, the elasticity of the primary materials ranged from 0.4 GPa to 0.9 GPa, but all of the mixed materials showed a stiffer behavior than the linear interpolation prediction, up to 57% above the prediction. The dimensions of the printed specimen were measured, and groups of different geometrical deviations were identified. These were analyzed with regard to the printer system and material mixture. In conclusion, this study shows and discusses the effects of the printing process on mechanical and dimensional properties of specimens fabricated using a stereolithographic 3D printer from multiple commercially available primary materials. It discusses a process for predicting the elastic properties of these multimaterials and selecting the mixing ratios to achieve specifically desired properties.

KEYWORDS

additive manufacturing, multimaterials, stereolithography, digital light processing, photopolymers, UV curing

1 Introduction

Additive manufacturing has rapidly gained popularity, both in industry and in academia, mainly because of the possibility of fabricating complex geometries in a relatively straightforward way. Currently, a wide range of different materials that can be manufactured, be it rigid or elastic polymers, metals, ceramics, or even comestibles (Lipton et al., 2015; Godoi et al., 2016; Maroni et al., 2017), are being proposed.

Recent studies have been investigating the effect of patterned surfaces and lattice structures to archive new designs through the so-called metamaterials, allowing the tuning of the mechanical properties of printed structures (Franco-Martínez et al., 2022; Han and Wei, 2022). Furthermore, new printing technologies employ materials responsive to various stimuli, such as temperature or electrical changes in the environment. This allows for the creation of complex geometries, otherwise not manufacturable, or functional structures, which can actively interact with their environment (Hann et al., 2020; Andreu et al., 2021). Not only is there a large selection of printable materials but also different printing methods (Stansbury and Idacavage, 2016). One of the most widespread manufacturing processes is stereolithography, which is the focus of this study. In this process, a liquid photopolymer is irradiated on a layer-by-layer basis, with UV light, which causes it to cure and therefore create structural stability. Stereolithography, often regarded as the pioneering 3D printing technique, involves scanning the intended printing layer with a laser (Su et al., 2018). In contrast, digital light processing (DLP) cures the entire layer at once by exposing the desired area through mirrors or a display. The concept and the printing materials used are basically the same; however, the two methods differ in printing time and printing result, depending on the available printer (Zhang et al., 2019; Unkovskiy et al., 2021).

So far, current research on DLP has focused mostly on the geometrical accuracy and surface finish properties but less on the mechanical properties of the printed parts. To create structures with adaptable dimensions, weight and precisely defined deflections under load materials have been developed to cover a range of elasticity (McKittrick et al., 2010). However, particularly, when it comes to mimicking a natural tissue or building prostheses and scaffolds for tissue engineering (Melchels et al., 2010), raw materials with suitable mechanical properties might not be available off the shelf.

It would therefore be advantageous to mix different base materials and obtain "intermediate" properties depending on their mixture ratios. Depending on the available printing system, the base materials can be mixed before or during the printing process (Tee et al., 2020; Jandyal et al., 2022). While the PolyJet technology relies on the mixture during the printing process and has been extensively investigated, the mixing of materials before printing and its effect on final mechanical properties have not been sufficiently investigated yet. The printing process also determines whether certain gradients of mixing ratios can be incorporated (Ituarte et al., 2019; Zhang et al., 2020; Niu et al., 2022).

Studies on material designing to reach certain material properties, e.g., by changing the composition of the photocurable resin, either by creating completely new material compositions or with additives in a preexisting material exist (Ligon et al., 2015; Borrello et al., 2018; Slapnik and Pulko, 2021). Moreover, the material properties depend on the properties of the polymer that influence curing, like the absorbance spectra, UV-light wavelength used, and temperature during fabrication (Fuh et al., 1999; Bennett, 2017; Hofstetter et al., 2018). Furthermore, some printers allow the modification of properties of the printed object via the printing process. For example, it is possible to use a photopolymer with two photoinitiators that cure at different exposure frequencies and produce structures with different stiffnesses (Cazin et al., 2022). However, especially in the case of photopolymers, where longer exposure times usually result in higher stiffnesses, it should be noted that the materials still undergo changes after the printing process. This property can be exploited during post-curing but must be taken into account when using the printed part since most photopolymers used currently react with UV components that are also present in daylight.

Most of the existing studies employ an experimental or simulative approach, and only a small number of publications deal with mathematical models that predict the properties of the 3D-printed parts, estimating the curing grade and the associated stiffness (Yang et al., 2019).

The present study deals with additively manufactured multimaterials and their respective elastic properties, particularly the effects of mixing ratios of commercially available resins on a range of elasticities, including the effects of post-curing. Specimens produced using an upside-down stereolithography 3D printer and their respective measurements and multimaterial prediction methods are shown. The chosen method includes blending of two primary materials before the initiation of the printing process, and therefore, homogeneous samples were obtained for each printed set of specimens. To the best of our knowledge, this is the first paper that investigates the elastic properties of these multimaterials and describes the mixing behavior in both the as-printed and post-cured states.

2 Materials and methods

2.1 Photopolymer SLA sample fabrication

All samples were fabricated with an *Anycubic Photon Mono* (Anycubic, Shenzhen, China) stereolithography 3D printer, with the same printing settings, as shown in Table 1, and in sets of 20

TABLE 1 Printing settings for Anycubic Photon Mono.

Property	Value
Resolution	1620 × 2560 px
Build area size	82.62 × 130.56 mm
Layer height	50 µm
Exposure time	2 s
Bottom layer count	6
Bottom exposure time	40 s
Light-off delay	0.5 s
Lifting distance	6 mm

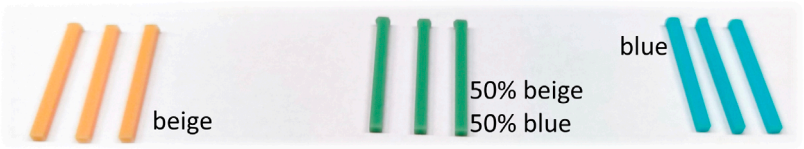

FIGURE 1
Photograph of *pure beige* and *blue* samples with one multimaterial. The size of each sample is 2×2.5×30 mm.

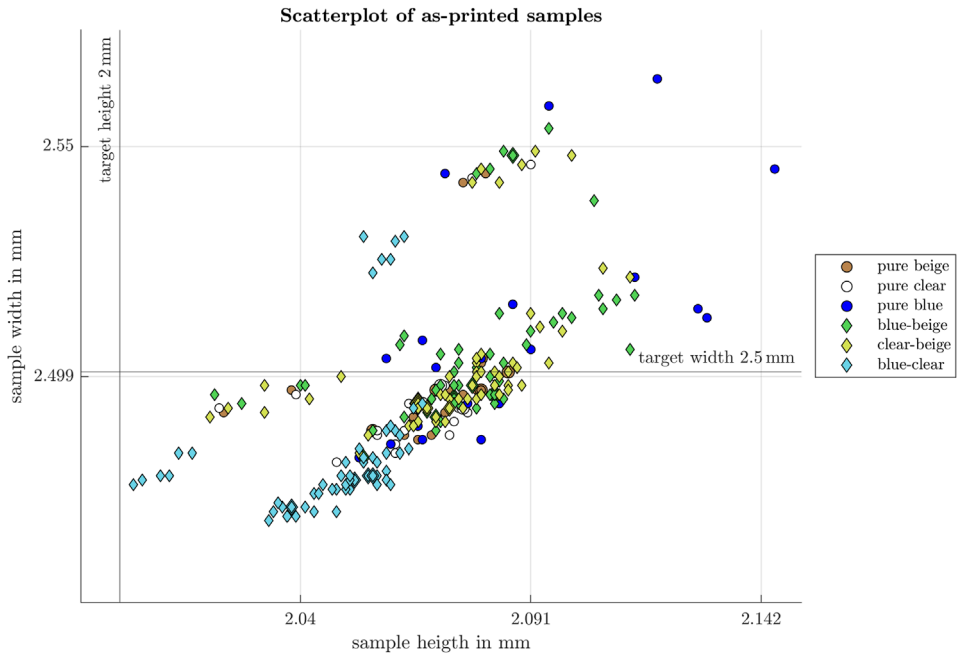

FIGURE 2
Scatterplot of as-printed samples. Width and height of 240 non-post-cured specimens. The nominal dimensions of the digital design are 2.5 mm width and 2 mm height. The grid represents the pixel sizes of the DLP display. No differences between the different mixture ratios are shown in the figure. Measurements were taken with a resolution of 1 µm, and specimens with the same sizes are represented with the markers of different sizes above each other.

specimens each. From three different photopolymers, a total of 480 samples were produced. The acrylic-based resins used were *craftsman beige*, *plant-based blue*, and *standard clear resin* (Anycubic, Shenzhen, China). The primary materials with different base components were selected, which led to different Young's moduli. For each resin, a reference set with the pure resin was fabricated, as well as three more specimen sets with each of the other resins, with the following mixture ratios: 25:75, 50:50, and 75:25. Mixing was carried out by hand in a beaker until a homogeneous resin was obtained.

This printer works with a vat and DLP. The slicer *CHITUBOX* (ChiTu Systems, Guangdong, China) was used to create a printable file from an STL geometry of the specimen. The same printing file was used for all prints, therefore, the specimens' positions on the building plate were identical. The models' dimensions are $2 \times 2.5 \times 30$ mm, and the specimens were printed vertically, meaning that the 2×2.5 mm surface of the specimen touches the building plate. The samples were randomly distributed across the build platform. Its cross-sectional area corresponds to the specimen size according to the 3-point bending tests of the DIN EN 843 standard.

Each material mixture was printed twice: one set of 20 samples was post-cured, while the other set of 20 samples was not. All specimens were washed in isopropyl alcohol and dried for 1 day before measurements. The hardened samples were post-cured for 30 min after the washing process in the UV-light polymerization unit *NextDent LC-3DPrint Box* (3D Systems, Rock Hill, United States). All machines were operated at a constant room temperature of 21.5°C ± 0.5°C.

2.2 Measurements

Dimensions of the specimen were measured using a *TESA Micromaster ø2mm* (Hexagon TESA, Renens, Switzerland) micrometer. The three-point bending measurements were

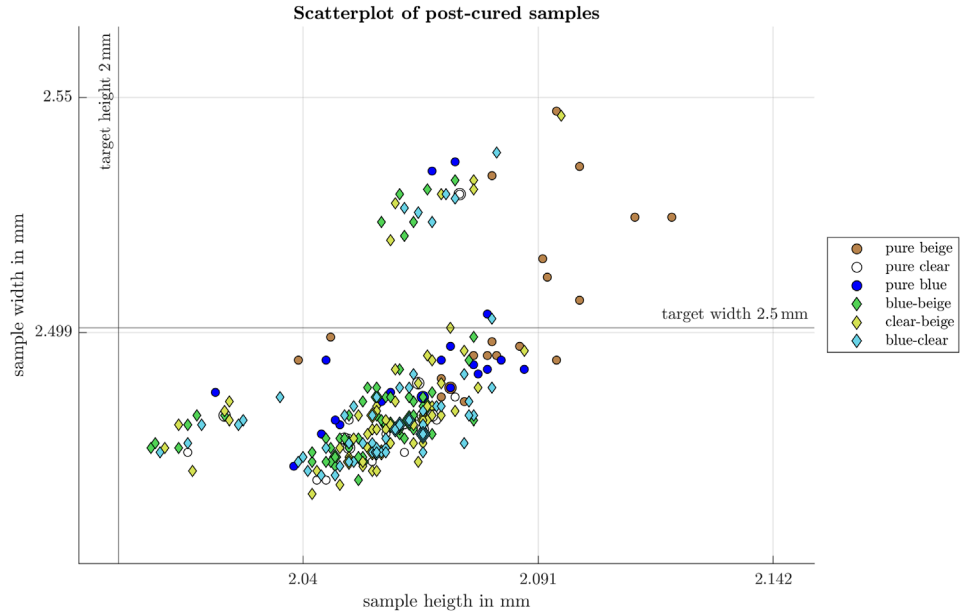

FIGURE 3
Scatterplot of post-cured samples. Width and height of 240 post-cured specimens. The nominal dimensions of the digital design are 2.5 mm width and 2 mm height. The grid represents the pixel sizes of the DLP display. No differences between the different mixture ratios are shown in the figure. Measurements were taken with a resolution of 1 µm, and specimens with the same sizes are represented with the markers of different sizes above each other.

performed using a *Messphysik BETA 10–2,5* (Messphysik GmbH, Fürstenfeld, Austria) universal tensile testing machine. The samples were placed on two cylinders (HRC 60) with a touch-point distance of 20 mm and a third cylinder loading the specimen from the top, similar to the standard DIN EN 834 (which is used for ceramic specimens with the same geometry). The feed rate was $v = 2.5\,\frac{\text{mm}}{\text{min}}$, and the maximum stroke was $l_{\text{max}} = 7$ mm. The room temperature was 21.5°C ± 0.5°C.

3 Results

3.1 Sample geometry

During fabrication, no misprints occurred. The selection of specimens is shown in Figure 1. The width and height of all printed non-post-cured specimen are shown in Figure 2, while the dimensions of the post-cured specimens are shown in Figure 3. Due to the limited resolution of 1 µm of the micrometer gauge, some dimensions appear to occur several times, which are indicated by larger, stacked markers.

Regarding the geometry, all sample sets showed two samples that are noticeably larger than the other samples, approximately the width of one pixel of the DLP display. The sample width was observed to be smaller or larger than the target width of 2.5 mm using the digital design, but no sample was below the target height of 2 mm.

3.2 Elasticity

All base materials have different Young's moduli, regardless of being post-cured or not. Young's moduli of the post-cured multimaterial samples ranged between those of the two base materials, where the material strength increases with the proportion of the harder material, as shown in Figure 4 for blue samples, clear samples, and their respective multimaterials. One exception to this scheme was the post-cured *25% clear/75% beige* samples (2230.7 ± 36.5 MPa) which exhibited a higher Young's modulus than that of pure post-cured *standard clear* resin (2183.1 ± 45.9 MPa, significant difference of the values, two-sample *t*-test *p*-value = 8.2×10^{-4}).

However, this simple scheme is not true for the non-post-cured specimen, where some mixtures show an even higher Young's modulus than that of the stiffer base material, as shown in Figure 4. No case was observed where the mean Young's modulus of a mixture was lower than that predicted by linearly interpolating the base materials with respect to the mixture volume fraction. All materials are listed with their respective Young's moduli in the Supplementary Data S1.

A comparison of the post-cured and non-post-cured samples is shown in Figure 4 for blue and clear photopolymers. Please refer to the Supplementary Data S1 for all other plots.

Assuming linear interpolation between the mean elastic properties of the primary materials to predict the elastic properties of the multimaterials as a model, the deviations of the measurement values from the model values are shown in Table 2. Herein, the deviation of each measurement value was compared to the predicted

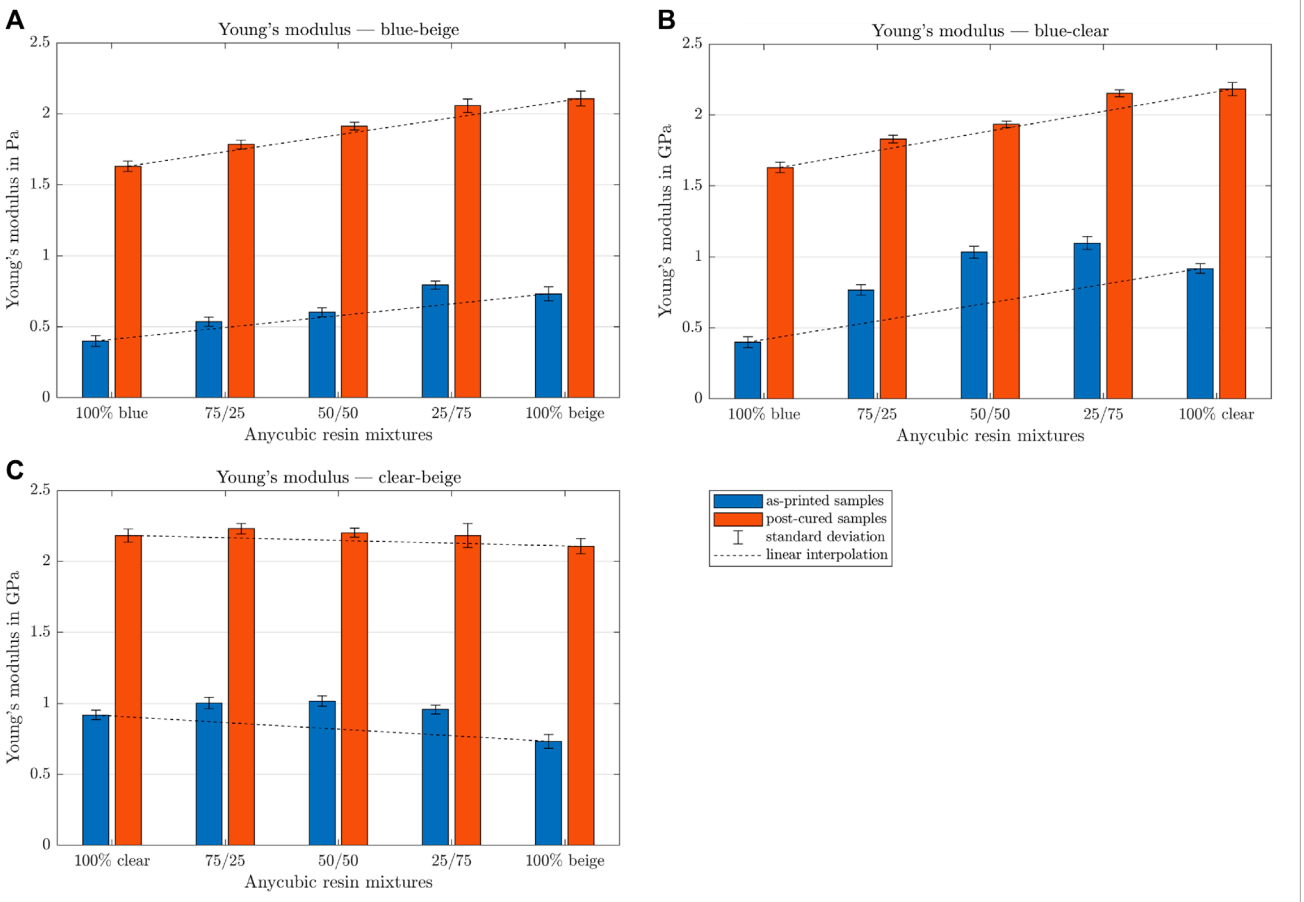

FIGURE 4
Comparison between the mean values of Young's moduli of samples fabricated from various mixtures of *standard clear*, *plant-based blue*, and *craftsman beige* photopolymers after 30 min in a post-curing chamber and as-printed samples of the same mixture. All materials become stiffer during the post-curing process. The dashed line shows the linear interpolation of the primary materials as a visual reference. **(A)** Young's modulus—blue beige; **(B)** Young's modulus—blue clear; **(C)** Young's modulus—clear beige.

value. Furthermore, the average of the measurement values was compared with the predicted value. Since the prediction uses the mean values of the primary materials, no difference exists between these values. In all cases, Young's moduli of the as-printed specimens deviated more from those predicted by linearly interpolating the primary materials than the post-cured specimens.

All breaks occurred in the center of the specimen, below the loading cylinder. Furthermore, all breaks were low-to-medium energy fractures, according to the DIN EN 843 standard. On average, the as-printed specimen ruptured at a higher strain. The respective load–strain curves are shown in the Supplementary Data S1.

4 Discussion

This study showed that as-printed and post-cured samples of mixed materials exhibit different behaviors related to the primary materials. The prediction by averaging the pure materials was within the range of the measurements for eight out of nine sample sets of the post-cured materials. However, the as-printed samples have a higher Young's modulus than that predicted by linearly interpolating the pure materials. This is most likely due to the different curing grades of the materials tested (Nowacki et al., 2021; Lang et al., 2022). In addition, there is likely to be a change in the cure behavior when the materials are mixed.

A relevant aspect of reliable and repeatable 3D printing processes is the geometric dimensions of the printed parts. The geometries of the samples show a quite stable process, although the placement on the build platform has to be considered, since the printer resolution is 51 µm per pixel. In addition to some scatter, a 51 µm difference represents the variation in sizes among certain specimens within the same sample set, with some being larger in one direction than others. Knowing that the size of the samples does not correspond to an integer number of pixels, the slicer software had to select one of the following numbers of pixels for the width: 48 px (2.448 mm), 49 px (2.499 mm), or 50 px (2.550 mm) and for the height: 39 px (1.989 mm), 40 px (2.040 mm), or 41 px (2.091 mm), not considering the possible pixel edges in the stated dimensions. Naturally, the size of the samples depends on the number of pixels that are switched on, which again depends on how the slicing software interprets the position on the building plate. This grouping on several used pixels can be well observed, particularly in the scatter plot of the post-cured specimen, as shown in Figure 3.

TABLE 2 Differences in the material properties of various mixtures according to the Young's modulus predicted by weighted averaging.

Percentage beige	Percentage blue	Percentage clear	Post-cured	Average difference in the linearly estimated Young's modulus	Difference in the average according to the linearly estimated Young's modulus
100	0	0	No	37.97 MPa (5.18%)	*Identical*
100	0	0	Yes	39.01 MPa (1.85%)	*Identical*
75	25	0	No	144.56 MPa (22.3%)	144.56 MPa (22.3%)
75	25	0	Yes	73.29 MPa (3.69%)	68.70 MPa (3.46%)
50	50	0	No	43.65 MPa (7.71%)	39.08 MPa (6.90%)
50	50	0	Yes	43.89 MPa (2.35%)	42.16 MPa (2.26%)
25	75	0	No	54.59 MPa (11.3%)	54.10 MPa (11.2%)
25	75	0	Yes	38.83 MPa (2.22%)	33.87 MPa (1.94%)
0	100	0	No	28.49 MPa (7.13%)	*Identical*
0	100	0	Yes	28.32 MPa (1.74%)	*Identical*
0	75	25	No	239.00 MPa (45.2%)	239.00 MPa (45.2%)
0	75	25	Yes	63.86 MPa (3.61%)	62.65 MPa (3.54%)
0	50	50	No	375.05 MPa (56.9%)	375.05 MPa (56.9%)
0	50	50	Yes	31.86 MPa (1.67%)	28.43 MPa (1.49%)
0	25	75	No	309.53 MPa (39.3%)	309.53 MPa (39.3%)
0	25	75	Yes	108.64 MPa (5.31%)	108.64 MPa (5.31%)
0	0	100	No	27.29 MPa (2.97%)	*Identical*
0	0	100	Yes	33.33 MPa (1.53%)	*Identical*
25	0	75	No	131.55 MPa (15.1%)	131.55 MPa (15.09%)
25	0	75	Yes	67.29 MPa (3.11%)	66.71 MPa (3.08%)
50	0	50	No	191.37 MPa (23.2%)	191.37 MPa (23.2%)
50	0	50	Yes	58.84 MPa (2.74%)	56.84 MPa (2.65%)
75	0	25	No	177.93 MPa (22.8%)	177.93 MPa (22.8%)
75	0	25	Yes	90.28 MPa (4.25%)	56.60 MPa (2.66%)

Due to the pixel alignment on the building platform, a correlation between the width and height could be observed. The correlation coefficient between the width and height of the specimens for all samples is $\rho_{all} = 0.5329$, while the correlation coefficients in the three groups are much higher: $\rho_1 = 0.8333, \rho_2 = 0.8942, \text{and} \rho_3 = 0.8329$. This indicates that the luminosity of the UV-light source is nonhomogeneous, and, therefore, some samples are more exposed than others, which results in larger geometric features.

Lastly, the geometry also depends on the light absorption and curing properties of the photopolymer itself; for example, the post-cured *pure beige* samples are on average larger than the post-cured *blue* samples ($h_{beige} = 2.0834 \pm 0.019$ mm > $h_{blue} = 2.0633 \pm 0.018$ mm, two-sample t-test p-value for non-equal means $p = 0.0015$).

Geometric mismatches due to the limited resolution in DLP stereolithography printers and the ill placement on the building plate can be treated in two ways. First, the positioning of identical geometries could be arranged with the same offset on the pixel grid of the matrix. However, this feature has to be supported during the slicing of the geometries. The slicer that comes with the printer, as well as most of the other freely available slicers, allows positioning on the building plate but does not offer information on pixels that are exactly turned on or off. Second, the pixels on the display are either activated or deactivated. Instead, employing pixels which are not fully illuminated (grayscale template) could enhance the overall geometry, both in terms of resolution (Zhou and Chen, 2012) and overhangs or rounded geometries (Mostafa et al., 2017; Guven et al., 2022).

Also important to consider before the fabrication is, that the elastic properties correlate with the curing state of the prints. The as-printed specimens seem not to have reached a fully cured state. This could explain the higher Young's moduli for multimaterials, assuming that these materials have reached an advanced curing state after printing compared to the pure materials. Particularly for the blue-clear mixtures, the multimaterials showed less change in the elastic properties during post-curing than the pure materials. The supplier

states a photoinitiator content of 2%–5%, and a higher photoinitiator content in the softer base material could explain the reason, why mixing with a harder base material results in a higher Young's modulus of the multimaterial, especially since this effect is not present in post-cured samples, where the remaining photoinitiator gets activated during the post-curing process. Considering this, a refined model for predicting mixed material properties would not only include the base materials and their mixing ratio but also include information about the fabrication process and curing status of the materials.

Measurements also showed that post-cured specimens are stiffer and have higher flexural strength but break at lower deflection. Central fractures without secondary fracture origins are an indicative of the materials being well mixed, meaning that coarse material transitions are not present in the sample.

5 Conclusion

In this study, multimaterials from DLP stereolithography 3D printing systems were investigated for their mechanical and geometrical properties. For DLP-printed multimaterials, where various primary materials are blended before the printing process, it is reasonable to assume linearly interpolated Young's moduli, particularly for fully cured 3D prints, which are typically employed. Only for some special applications, where non-post-cured samples are used, one needs to find a different material model or print some samples for preliminary tests. Since the material properties are not dependent on how the resin is exposed to UV light, these findings are expected to be generalizable to other types of SLA printers but not to other printing methods.

A large number of measurements of different materials have been recorded. These results lay a foundation for further studies to create elaborate simulation and prediction models for multimaterial stereolithography 3D printing. Precise predictions and planning of 3D-printed elastic properties will allow the fabrication of individualized and optimized substitutes, like tailored prostheses in healthcare or equipment adapted for athletes in professional sports.

Data availability statement

The original contributions presented in the study are included in the article/Supplementary Material; further inquiries can be directed to the corresponding author.

Author contributions

EK: data curation, investigation, methodology, validation, visualization, writing-original draft, and writing-review and editing. MK: resources and writing-review and editing. EU: resources and writing-review and editing. FM: funding acquisition, supervision, and writing-review and editing.

Funding

The author(s) declare financial support was received for the research, authorship, and/or publication of this article. Funding was provided by the Austrian Research Promotion Agency (FFG): INKplant Project Nr. 877452.

Acknowledgments

The computational results presented have been achieved in part using the Vienna Scientific Cluster (VSC-4). The authors would like to thank Andreas Hodul for his invaluable assistance in setting up the measurement equipment. The authors would also like to acknowledge and appreciate Elise Scheiber's valuable contribution to enhancing the language and clarity of this article.

Conflict of interest

The authors declare that the research was conducted in the absence of any commercial or financial relationships that could be construed as a potential conflict of interest.

The author(s) declared that they were an editorial board member of Frontiers, at the time of submission. This had no impact on the peer review process and the final decision.

Publisher's note

Supplementary material

The Supplementary Material for this article can be found online at: https://www.frontiersin.org/articles/10.3389/fmats.2023.1272147/full#supplementary-material

References

Andreu, A., Su, P. C., Kim, J. H., Ng, C. S., Kim, S., Kim, I., et al. (2021). 4d printing materials for vat photopolymerization. *Addit. Manuf.* 44, 102024. doi:10.1016/j.addma.2021.102024

Bennett, J. (2017). Measuring uv curing parameters of commercial photopolymers used in additive manufacturing. *Addit. Manuf.* 18, 203–212. doi:10.1016/j.addma.2017.10.009

Borrello, J., Nasser, P., Iatridis, J. C., and Costa, K. D. (2018). 3d printing a mechanically-tunable acrylate resin on a commercial dlp-sla printer. *Addit. Manuf.* 23, 374–380. doi:10.1016/j.addma.2018.08.019

Cazin, I., Gleirscher, M. O., Fleisch, M., Berer, M., Sangermano, M., and Schlögl, S. (2022). Spatially controlling the mechanical properties of 3d printed objects by dual-wavelength vat photopolymerization. *Addit. Manuf.* 57, 102977. doi:10.1016/j.addma.2022.102977

Franco-Martínez, F., Grasl, C., Kornfellner, E., Vostatek, M., Cendrero, A. M., Moscato, F., et al. (2022). Hybrid design and prototyping of metamaterials and metasurfaces. *Virtual Phys. Prototyp.* 17, 1031–1046. doi:10.1080/17452759.2022.2101009

Fuh, J., Lu, L., Tan, C., Shen, Z., and Chew, S. (1999). Curing characteristics of acrylic photopolymer used in stereolithography process. *Rapid Prototyp. J.* 5, 27–34. doi:10.1108/13552549910251855

Godoi, F. C., Prakash, S., and Bhandari, B. R. (2016). 3d printing technologies applied for food design: status and prospects. *J. Food Eng.* 179, 44–54. doi:10.1016/j.jfoodeng.2016.01.025

Guven, E., Karpat, Y., and Cakmakci, M. (2022). Improving the dimensional accuracy of micro parts 3d printed with projection-based continuous vat photopolymerization using a model-based grayscale optimization method. *Addit. Manuf.* 57, 102954. doi:10.1016/j.addma.2022.102954

Han, Z., and Wei, K. (2022). Multi-material topology optimization and additive manufacturing for metamaterials incorporating double negative indexes of Poisson's ratio and thermal expansion. *Addit. Manuf.* 54, 102742. doi:10.1016/j.addma.2022.102742

Hann, S. Y., Cui, H., Nowicki, M., and Zhang, L. G. (2020). 4d printing soft robotics for biomedical applications. *Addit. Manuf.* 36, 101567. doi:10.1016/j.addma.2020.101567

Hofstetter, C., Orman, S., Baudis, S., and Stampfl, J. (2018). Combining cure depth and cure degree, a new way to fully characterize novel photopolymers. *Addit. Manuf.* 24, 166–172. doi:10.1016/j.addma.2018.09.025

Ituarte, I. F., Boddeti, N., Hassani, V., Dunn, M. L., and Rosen, D. W. (2019). Design and additive manufacture of functionally graded structures based on digital materials. *Addit. Manuf.* 30, 100839. doi:10.1016/j.addma.2019.100839

Jandyal, A., Chaturvedi, I., Wazir, I., Raina, A., and Ul Haq, M. I. (2022). 3d printing – A review of processes, materials and applications in industry 4.0. *Sustain. Operations Comput.* 3, 33–42. doi:10.1016/j.susoc.2021.09.004

Lang, M., Hirner, S., Wiesbrock, F., and Fuchs, P. (2022). A review on modeling cure kinetics and mechanisms of photopolymerization. *Polymers* 14, 2074. doi:10.3390/polym14102074

Ligon, S., Schwentenwein, M., Gorsche, C., Stampfl, J., and Liska, R. (2015). Toughening of photo-curable polymer networks: A review. *Polym. Chem.* 7. doi:10.1039/C5PY01631B

Lipton, J. I., Cutler, M., Nigl, F., Cohen, D., and Lipson, H. (2015). Additive manufacturing for the food industry. *Trends Food Sci. Technol.* 43, 114–123. doi:10.1016/j.tifs.2015.02.004

Maroni, A., Melocchi, A., Parietti, F., Foppoli, A., Zema, L., and Gazzaniga, A. (2017). 3d printed multi-compartment capsular devices for two-pulse oral drug delivery. *J. Control. Release* 268, 10–18. doi:10.1016/j.jconrel.2017.10.008

McKittrick, J., Chen, P. Y., Tombolato, L., Novitskaya, E., Trim, M., Hirata, G., et al. (2010). Energy absorbent natural materials and bioinspired design strategies: A review. *Mater. Sci. Eng. C* 30, 331–342. doi:10.1016/j.msec.2010.01.011

Melchels, F. P., Feijen, J., and Grijpma, D. W. (2010). A review on stereolithography and its applications in biomedical engineering. *Biomaterials* 31, 6121–6130. doi:10.1016/j.biomaterials.2010.04.050

Mostafa, K., Qureshi, A. J., and Montemagno, C. (2017). "Tolerance control using subvoxel gray-scale DLP 3d printing," in ASME 2017 International Mechanical Engineering Congress and Exposition, Tampa, Florida, USA, November 3–9, 2017. doi:10.1115/IMECE2017-72232.V002T02A035

Niu, C., Luan, C., Shen, H., Song, X., Fu, J., Zhang, L., et al. (2022). Tunable soft–stiff hybridized fiber-reinforced thermoplastic composites using controllable multimaterial additive manufacturing technology. *Addit. Manuf.* 55, 102836. doi:10.1016/j.addma.2022.102836

Nowacki, B., Kowol, P., Kozioł, M., Olesik, P., Wieczorek, J., and Wacławiak, K. (2021). Effect of post-process curing and washing time on mechanical properties of msla printouts. *Materials* 14. doi:10.3390/ma14174856

Slapnik, J., and Pulko, I. (2021). Tailoring properties of photopolymers for additive manufacturing with mixture design. *Prog. Addit. Manuf.* 6, 83–91. doi:10.1007/s40964-020-00147-1

Stansbury, J. W., and Idacavage, M. J. (2016). 3d printing with polymers: challenges among expanding options and opportunities. *Dent. Mater.* 32, 54–64. doi:10.1016/j.dental.2015.09.018

Su, A., and Al'Aref, S. J. (2018). "Chapter 1 - history of 3d printing," in *3D printing applications in cardiovascular medicine*. Editors S. J. Al'Aref, B. Mosadegh, S. Dunham, and J. K. Min (United States: Academic Press), 1–10. doi:10.1016/B978-0-12-803917-5.00001-8

Tee, Y. L., Peng, C., Pille, P., Leary, M., and Tran, J. P. (2020). Polyjet 3d printing of composite materials: experimental and modelling approach. *JOM J. Minerals, Metals Mater. Soc.* 72, 13. doi:10.1007/s11837-020-04014-w

Unkovskiy, A., Schmidt, F., Beuer, F., Li, P., Spintzyk, S., and Kraemer Fernandez, P. (2021). Stereolithography vs. direct light processing for rapid manufacturing of complete denture bases: an *in vitro* accuracy analysis. *J. Clin. Med.* 10. doi:10.3390/jcm10051070

Yang, Y., Li, L., and Zhao, J. (2019). Mechanical property modeling of photosensitive liquid resin in stereolithography additive manufacturing: bridging degree of cure with tensile strength and hardness. *Mater. Des.* 162, 418–428. doi:10.1016/j.matdes.2018.12.009

Zhang, X., hui Chueh, Y., Wei, C., Sun, Z., Yan, J., and Li, L. (2020). Additive manufacturing of three-dimensional metal-glass functionally gradient material components by laser powder bed fusion with *in situ* powder mixing. *Addit. Manuf.* 33, 101113. doi:10.1016/j.addma.2020.101113

Zhang, Zc, Li, Pl, Chu, Ft, and Shen, G. (2019). Influence of the three-dimensional printing technique and printing layer thickness on model accuracy. *J. Orofac. Orthop.* 80, 194–204. doi:10.1007/s00056-019-00180-y

Zhou, C., and Chen, Y. (2012). Additive manufacturing based on optimized mask video projection for improved accuracy and resolution. *J. Manuf. Process.* 14, 107–118. doi:10.1016/j.jmapro.2011.10.002